Full length article

Mechanics and properties of fish fin rays in nonlinear regimes of large deformations

Saurabh Das[a], Florent Hannard[b], Francois Barthelat[a,*]

[a] *Department of Mechanical Engineering, University of Colorado, 427 UCB, 1111 Engineering Dr, Boulder, CO 80309, USA*
[b] *Institute of Mechanics, Materials and Civil Engineering, UCLouvain, Louvain-la-Neuve, Belgium*

A R T I C L E   I N F O

A B S T R A C T

Fins from ray-finned fishes do not contain muscles, yet fish can change the shape of their fins with high precision and speed, while producing large hydrodynamic forces without collapsing. This remarkable performance has been intriguing researchers for decades, but experiments have so far focused on homogenized properties, and models were developed only for small deformations and small rotations. Here we present fully instrumented micromechanical tests on individual rays from Rainbow trout in both morphing and flexural deflection mode and at large deflections. We then present a nonlinear mechanical model of the ray that captures the key structural elements controlling the mechanical behavior of rays under large deformations, which we successfully fit onto the experiments for property identification. We found that the flexural stiffness of the mineralized layers in the rays (hemitrichs) is 5-6 times lower than their axial stiffness, an advantageous combination to produce stiff morphing. In addition, the collagenous core region can be modeled with spring elements which are 3-4 orders of magnitude more compliant than the hemitrichs. This fibrillar structure provides negligible resistance to shearing from the initial position, but it prevents buckling and collapse of the structure at large deformations. These insights from the experiments and nonlinear models can serve as new guidelines for the design of efficient bioinspired stiff morphing materials and structures at large deformations.

Statement of significance

Fins from ray-finned fishes do not contain muscles, yet fish can change the shape of their fins with high precision and speed, while producing large hydrodynamic forces without collapsing. Experiments have so far focused on homogenized properties, and models were developed only for small deformations and small rotations providing limited insight into the rich nonlinear mechanics of natural rays. We present micromechanical tests in both morphing and flexural deflection mode on individual rays, a nonlinear model of the ray that captures the mechanical behavior of rays under large deformations and combine microCT measurements to generate new insights into the nonlinear mechanics of rays. These insights can serve as new guidelines for the design of efficient bioinspired stiff morphing materials and structures at large deformations.

1. Introduction

Ray-finned fishes (Actinopterygii) are the most common type of fish on earth, and they represent more than half of all vertebrate species. This evolutionary success is due to their exceptional agility, speed and swimming efficiency, and to the remarkable construction of their fins. Fish fins from Actinopterygii do not contain muscles but display large morphing amplitudes, combined with high stiffness from external loads (such as hydrodynamic forces), fast response times and localized actuation forces from the base of the fin only. Fish fin "probably represents the most elaborate and refined adaptation to efficient interaction with water that has ever evolved" [1] and as such, they can serve as models for the design of new morphing materials. Since fish fins are semi-flexible membranes which contain no muscles, they are often thought of as passive swimming surfaces which are simply "flapped" for propulsion (caudal fin) or for passive stabilization (dorsal fin, caudal fins). Fish fins are in fact much more sophisticated systems: Fish can adjust not only the orientation, but also the curvature, shape, and surface of their fins to finely tune their hydrodynamic interactions and to

* Corresponding author.
  E-mail address: francois.barthelat@colorado.edu (F. Barthelat).

generate powerful forces in three dimensions (Fig. 1a, [2]). Individual fish fins are composed of a collagenous membrane stiffened by 10-30 beam-like structures called rays. Each ray has a diameter in the order of ~100 μm with a tapered profile and an aspect ratio > 100 (Fig. 1b). The rays are composed of two bony layers called hemitrichs which are connected by collagen fibrils embedded in ground gel-like substance (Fig. 1c). A prominent feature of the hemitrichs is their segmentation into ~300 μm bony segments.

A remarkable feature of fish fins is that their curvature can be adjusted solely by muscular actuation from the base of the rays (Fig. 1a, d). Push/pull actuation induces shear deformations in the core region, while rotations at the base are prevented by the configuration of the tendons and by a cartilaginous pad at the base of the fin [3]. The shear deformation imposed at the base of the core progressively translates into flexural deflection over a length scale governed by the structure and the mechanical properties of the constituents of the ray. For proper and uniform morphing, this "morphing length" must match the length of the fin. There is a fine balance between the flexural stiffness of the hemitrichs and the shear stiffness of the core, so that individual rays can morph along their entire length [3–5]. A core region which is too stiff relative to the hemitrichs would lead to localized deformations and a "hinge" at the base of the fin. In contrast, a core region which is too compliant relative to the hemitrichs would lead to the uniform shearing of the entire core region, with no flexural deformations in the hemitrichs and therefore no morphing. Individual rays must also be stiff to minimize deformations and prevent collapse when subjected to hydrodynamic loads. Flexural experiments on individual rays have indeed revealed relatively high flexural stiff-

ness, with homogenized flexural modulus in the order of 1 GPa [6] (for comparison, synthetic materials with large morphing amplitudes are orders of magnitude softer). Also interestingly, flexural deflections from hydrodynamic forces in fish fins can be compensated by applying actuation forces at the base of the fins. Therefore fish fins have an "active", tunable flexural stiffness which can be adjusted from the base muscles [3]. In effect, fish can cancel deflections from external loads, thereby tuning their apparent stiffness to infinity.

Fish fins therefore represent an elegant, robust and mechanically efficient solution to stiff morphing. In comparison, engineering morphing materials are either highly deformable and compliant, or stiff but with little morphing amplitudes. This design contradiction severely limits their range of applications (Fig. 1f). A wide range of technologies are available for engineering morphing materials: metamaterials [7–9], origami [10], kirigami [11], hydrogels [12], hygromorphs [13], pneumatic shape-morphing elastomers [14,15]. Radical shape change is achieved in these materials, but only with relatively soft materials and structures that cannot sustain large external forces without excess deformations, collapse or failure. In contrast, stiff and strong structures can be morphed using piezoelectric actuators [16] or shape memory alloys [17], but large actuation forces are required and only relatively small morphing amplitudes are achieved. This conflict between "morphing efficiency" and stiffness from external loads has been a major obstacle to the systematic use of morphing materials in aerospace and other domains [18] (Fig. 1f).

A better understanding of the finely tuned architecture and mechanics of fin rays could therefore inspire new design strategies for stiff morphing materials that overcome these limitations.
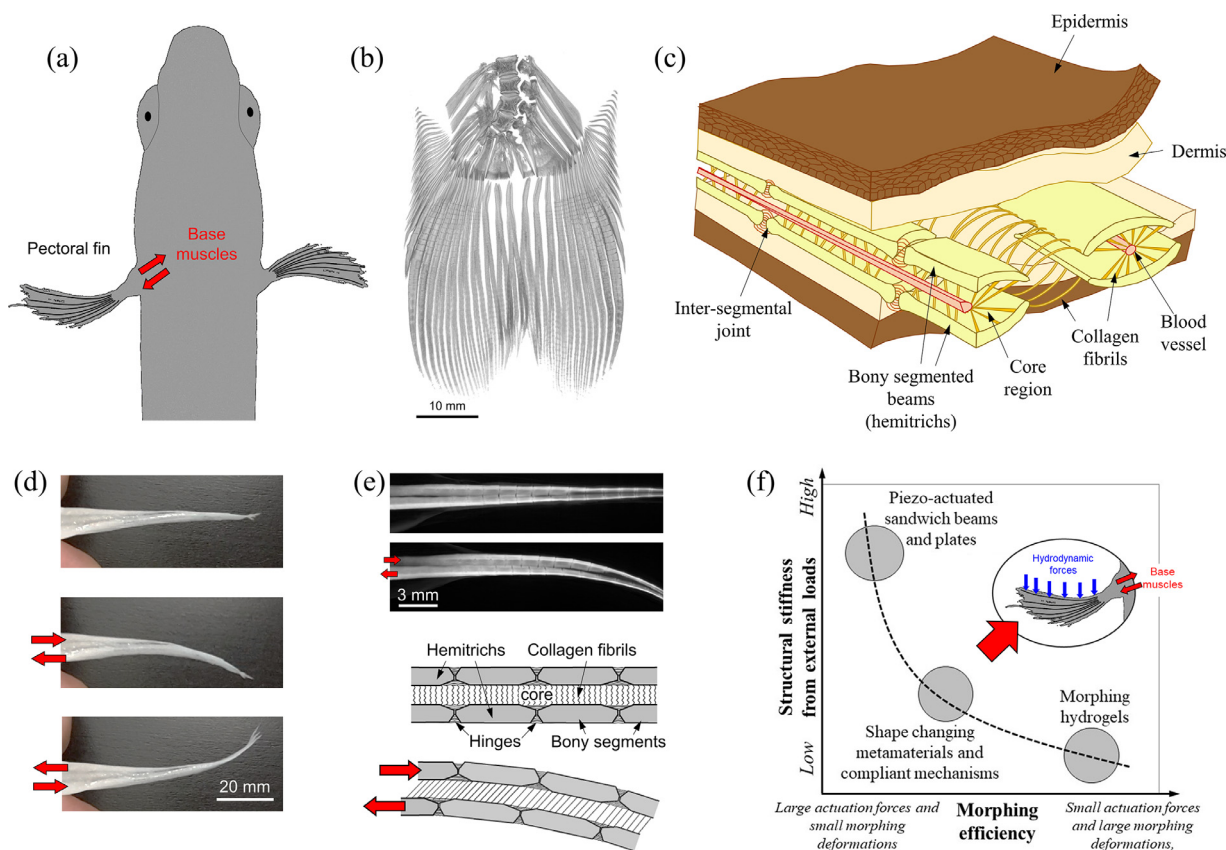

Fig. 1. Key features in individual fin rays: (a) Fish can change the shape and effective surface of their fins from actuation by base muscles (Adapted from [3]) (b) MicroCT of a caudal fin from Rainbow trout (*Oncorhynchus mykiss*); (c) Cross section of a fin showing the bony rays and surrounding softer tissues; (d) An individual ray from a fish fin harvested from Atlantic salmon (*Salmo salar*) is "morphed" by applying push/pull forces manually; (e) schematic of this mechanism; (f) Fish fins combine high morphing efficiency and high stiffness from external loads, two properties that are mutually exclusive in engineering morphing materials.

Despite the importance of fin rays on fish locomotion [19,20] and their remarkable mechanical performance in terms of mechanics and fluid-structure interactions [21–23], there are still large gaps in our understanding of structure-performance-function relationships in this key vertebrate structure, especially at regimes of large deformations [24]. Morphing tests were performed in individual rays [3,4,24,25], but they most often only focus on curvature analysis and deflection, with no data on actuation force. Flexural tests were also performed on individual rays [23,26–28], but they only reported homogenized modulus that ignored the fine structure of the ray and do not consider the properties of core region and hemitrichs independently. Finally, mechanical models were proposed for individual rays [3–5], but only in the linear regimes of deformation and material properties, providing only a small insight into the rich nonlinear interplays between core and hemitrichs. Other classes of models homogenize the entire ray into a single foil, which can be modeled using a flexible multi-segment idealization [23]. These models are useful to optimize the properties of passive fins and their interaction with fluids, but they do not inform morphing performance nor the properties of the individual structural components of the fin. The mechanical properties of hemitrichs and core regions could only be estimated from scaling arguments, from other collagenous materials or similar mineralized tissues, or from cross-sectional geometries [3,4,26]. Here we present fully instrumented micromechanical tests in both morphing and deflection modes on individual rays from Rainbow trout, followed by a nonlinear mechanical model of the ray that captures the main structural and mechanical features of rays at large deformations. The model and experiments are then analyzed in detail to produce new insight into the nonlinear mechanics of individual rays.

2. Experiments

We harvested individual rays from the caudal fins of fresh specimens of Rainbow Trout (*Oncorhynchus mykiss*, Liley Fisheries Inc, Boulder, Colorado). The specimens ranged from 12" to 20" in length. We carefully snipped the caudal fin to ensure that a sizeable portion of the fish muscles were also attached to the fin. The caudal fin was then transferred to a dissection plate and the fin rays were carefully isolated using a surgical knife to prevent damage to the bony hemitrichs and the collagenous core. The samples were then frozen until testing (we found that freezing and thawing had minimal effect on the mechanical response of the ray). Fig. 2a shows a typical microCT of the caudal fin, obtained on a Phoenix Nanotom M (GE Measurement and Control Solutions, Germany) with an isotropic voxel size of 17 μm. Several acquisitions with "stack" scanning strategy were performed to image the entire ray with an isotropic voxel size of 2 μm (Fig. 2b). The fin is composed of about 20-30 rays. Each fin ray is about 45 – 60 mm long, with a cross section in the order of 3×3 mm^2 at the base of the ray, and decreasing towards the end of ray. Closer examination from the microCT data (Fig. 2b) shows that this tapered geometry is both due to a decrease in the thickness of the collagenous core region, and to a decrease in the cross-section area of the hemitrichs from the base to the end of the ray. In addition, individual rays start branching about half-way along their length.

Mechanical tests: Each ray was subjected to two types of tests: a "cantilever test" to measure the flexural stiffness of the ray under an external transverse force and a "morphing test" where the ray was subjected to push/pull displacements at the base. Fig. 3 shows the custom experimental platform we developed for these tests. Individual rays were attached at their base using two clamps. One
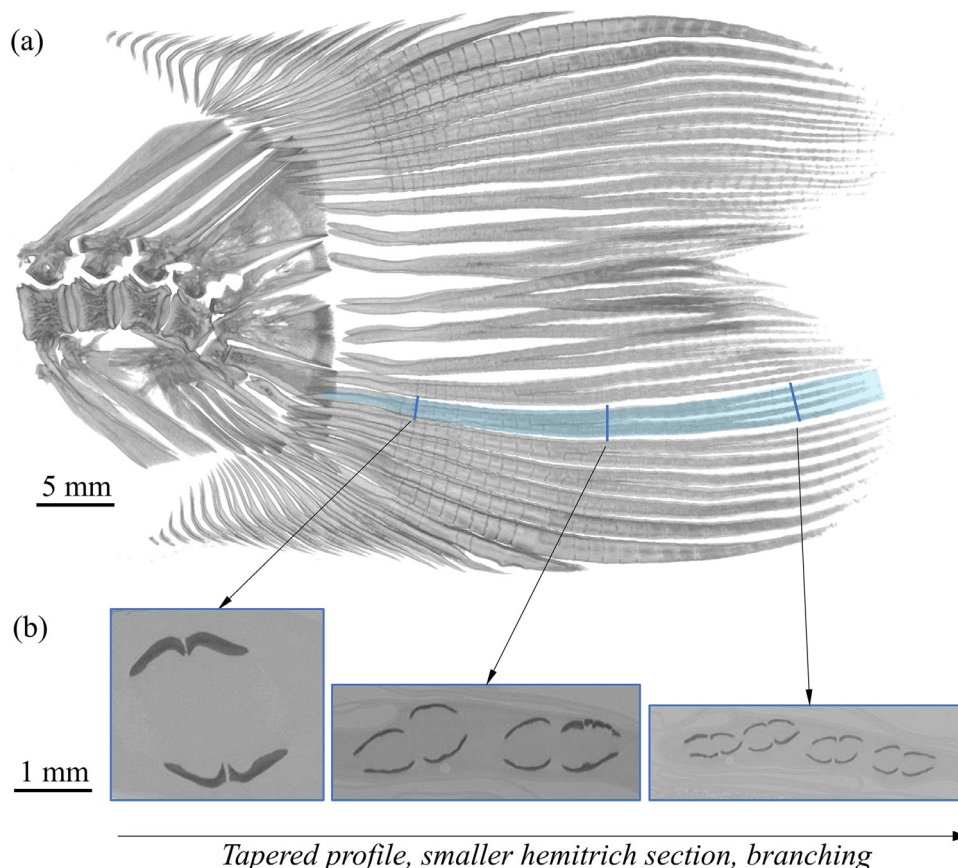

Tapered profile, smaller hemitrich section, branching

Fig. 2. (a) MicroCT scan of a caudal fin from rainbow trout; (b) Cross sections taken at three different places along the length of a ray show a decrease in overall cross section, a decrease in the cross section of the hemitrichs, and branching.
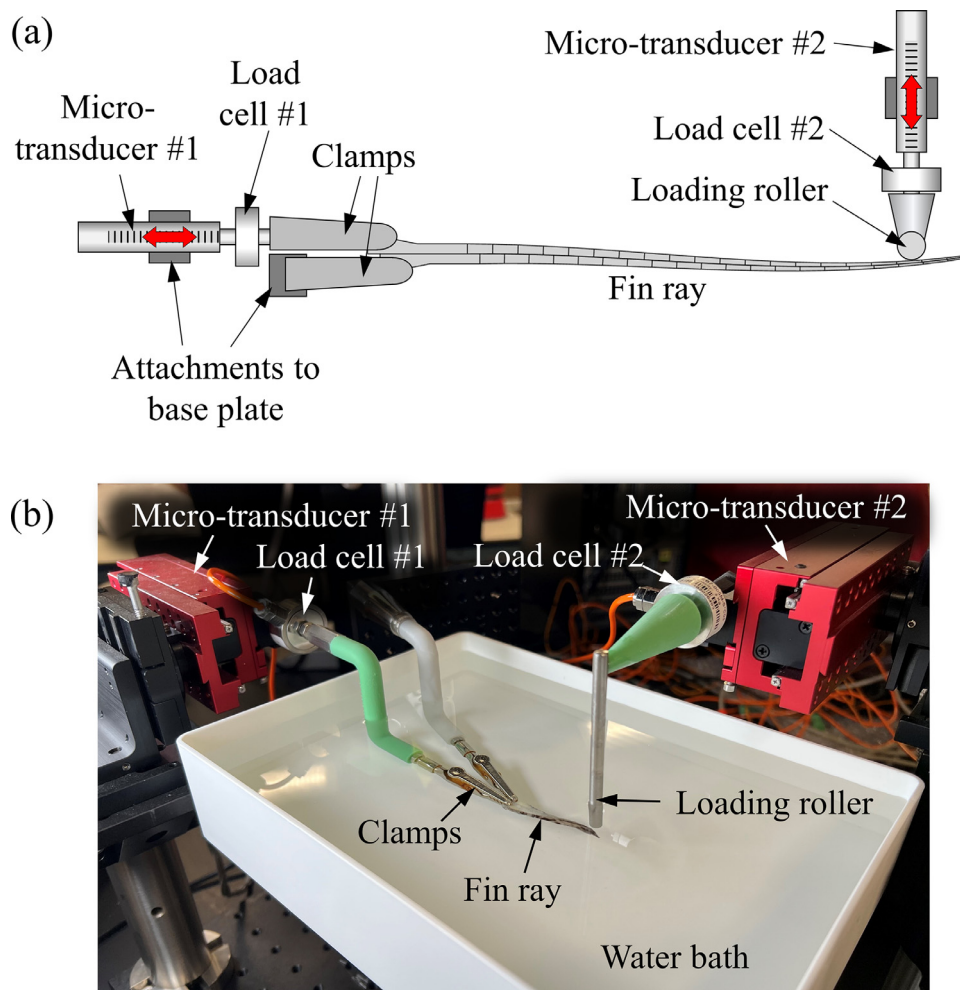
Fig. 3. (a) Schematic of experimental setup used in our research study. (b) Assembly of the experimental setup based on the schematic.

of the clamps was attached to a fixed position, while the other clamp was mounted in line with a motorized micro-transducer (SOLO Single Axis Manipulator Controller, Sutter Instrument, CA, USA), and a precision 5 kg load cell (REB7 Subminiature Load Cell, 5 kg capacity, Loadstar Sensors). The clamping force applied on the base of the ray was firm enough to prevent slippage and rotation, while gentle enough not to crush the base of the hemitrichs. During the test, the ray was entirely immersed in a bath of water to prevent sample desiccation (Fig. 3b). For the morphing tests, a controlled actuation displacement u_0 was applied at the base of the ray to emulate the action of the muscles, while the actuation force F_0 was measured. A calibrated digital camera was used to acquire images of the ray at regular time intervals during the test. A typical morphing test consisted of a "push" of the hemitrich base at a rate of 10 μm/sec and up to a maximum of about 2 mm. The hemitrich was then pulled back at the same rate, past the rest position and onto the other side, up to 2 mm. Each ray was then immediately tested for "cantilever" loading. In this configuration both bases of the hemitrichs were maintained in a fixed position, and a second motorized micro-transducer placed and oriented transversely to the axis of the ray was used to deflect the ray by a controlled distance δ, while the corresponding transverse force P was recorded with a precision load cell in line with the transducer. The ray was deflected at a rate of 10 μm/sec and up to a maximum of about 10 mm, selected to cover both the linear and the nonlinear regimes but without damage to the rays.

Fig. 4 shows typical results of the flexural tests and the morphing tests on three rays, color coded with red, blue and green

(Fig. 4a). Each ray was subjected to cantilever and morphing tests. The cantilever tests (Fig. 4b) showed a relatively linear loading, with only a slight stiffening in some cases. The unloading shows hysteresis, indicating some form of dissipative process. At the slow deformation rate of the mechanical tests presented here, drag forces from the water on the ray are negligible, and a more likely explanation is the viscoelastic character of the collagenous regions (core region, hinges in the hemitrichs, surrounding dermal tissues). Additional loading-unloading tests on the same ray yielded repeatable results, indicating that no damage accumulation occurred during the test. Fig. 4c, Fig. 4d show the results from the morphing tests on the same three rays. We used a custom MATLAB image analysis code to track the shape of the deformed ray (morphing elastica) at different levels of actuation. As expected, the push/pull action at the base of the ray induces a change of curvature along the ray (Fig. 4c), with large deformations and rotations. Fig. 4d shows the corresponding actuation force-displacement response (F_0-u_0 curve). The actuation force increases with actuation displacement, and the response is almost symmetric in tension and compression for the actuation displacement. There are however pronounced nonlinear features: The response is initially linear, with a relatively low stiffness in the order of 0.01 N/mm. Near the rest position of the fin, the ray therefore offers very little resistance to actuation, so it is relatively "easy" to initiate morphing. However, the response stiffens significantly at about $u_0 = 0.5$-1 mm, to about 1-2 N/mm. This non-linear response could serve as a "fail-safe" mechanism to protect the ray from overloading, or it could promote a "tendon effect" [29] which could improve the efficiency
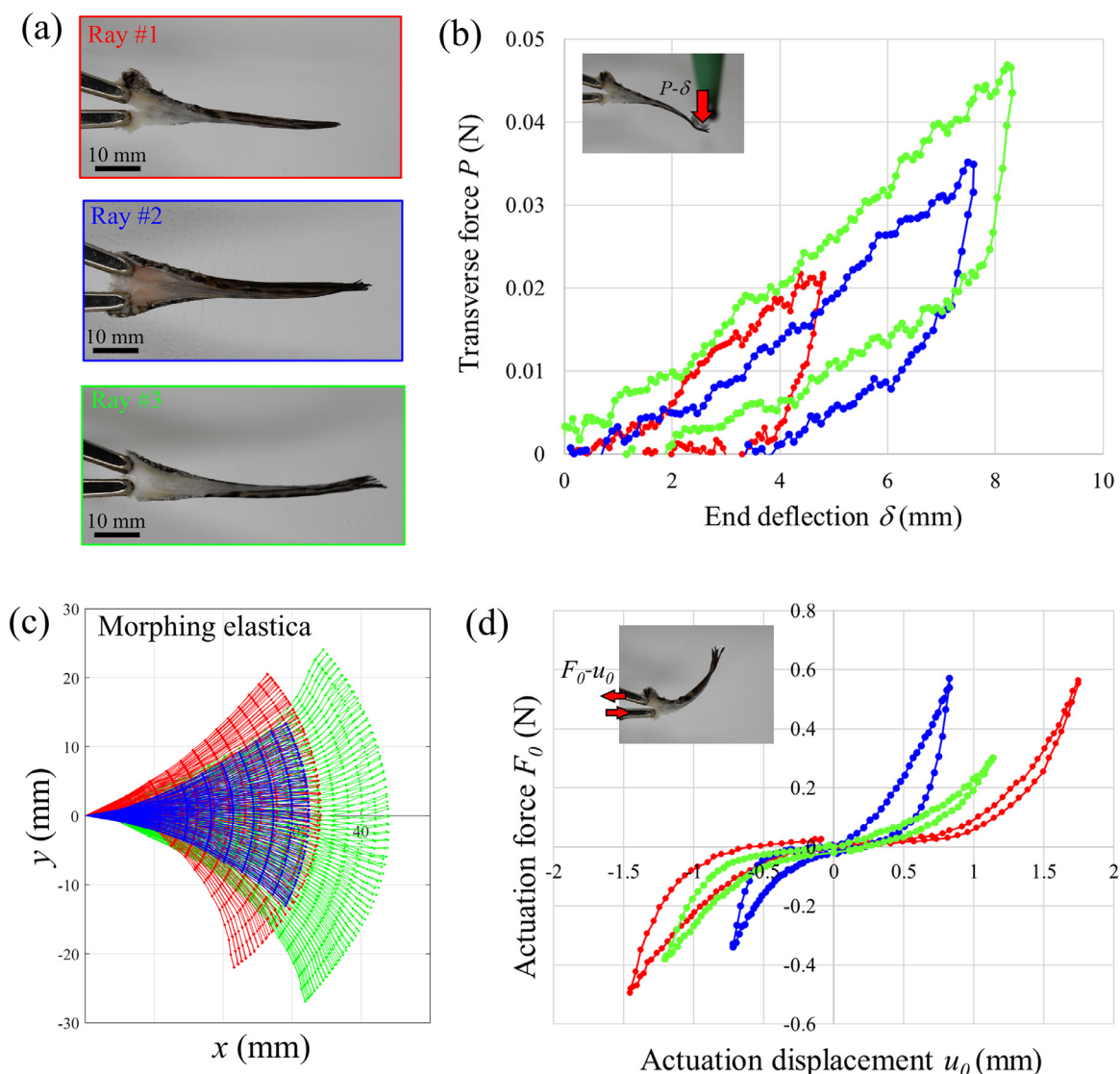
Fig. 4. Typical results for mechanical tests showed for three rays: (a) The rays varied in dimensions; (b) P-d curves from the cantilever flexural test; Results from the morphing tests: (c) elastica extracted from image analysis and (d) F_0- u_0 curves. The results showed significant variability across samples.

of morphing and swimming. In terms of mechanics, this behavior could be due to geometric nonlinearities, material nonlinearities, or both (we investigate these possibilities below). The F_0-u_0 loading-unloading cycles also show some hysteresis, again probably due to the viscoelastic response of the softer components. Finally, multiple cycles performed on the same ray showed no decrease in stiffness and morphing amplitudes, indicating that the range of actuation displacement we chose did not induce any damage in the ray.

Fig. 4 show typical results which also demonstrate an important point: Individual rays, even if they are harvested from the same fin, show significant variability in terms of dimensions and in terms of mechanical response. This has represented a significant barrier to accurate and repeatable measurements of properties [6,28,30]. In addition, the mechanical responses shown on Fig. 4 result from a relatively complex structure made of hard bony segments, hinges, collagen fibrils and other soft tissues. Our attempts to further "deconstruct" individual rays into their individual components for mechanical testing without disrupting their properties were not successful. For example, the core region of the ray can be ablated from the ray, but this involves the sectioning of the collagen fibrils in the core, which greatly affects any measurement of me-

chanical properties. We also separated the two hemitrichs by cutting through the core regions, but attempts at mechanical tests on individual hemitrichs were unreliable because of the damage created in the process. We also excluded other local measurements of modulus such as nanoindentation. The hemitrichs and core are composed of anisotropic materials which complicates the interpretation of nanoindentation data. In addition, nanoindentation would make it difficult to achieve large deformations in the ray. We therefore took another approach for this study, where we sought to identify the properties of hemitrichs and core regions using only the experiments shown on Fig. 4, since they duplicate the loading modes that the ray experiences in normal conditions. For this purpose we developed a nonlinear mechanical model which we used for property identification, and also to explore some of the main mechanisms of rays in the nonlinear range.

3. A nonlinear model for individual rays

Previous mechanical models for rays developed by our group and others used linear analysis only [3–5]. The materials were assumed to follow linear elasticity, and small deformations and small rotations were assumed. Our attempts to approach our

experiments with these linear models were unsuccessful. Considering the large rotations of the ray during morphing, and the large shear strains (>100%) in the collagenous core regions, linear approaches are not appropriate and nonlinear models that at least capture geometric nonlinearities are required. We therefore sought a relatively simple but robust nonlinear model that captures the main structural features of individual rays, as well as their key deformation mechanisms and properties. In particular we were interested in a model accurate enough to duplicate the experiments, and to capture the mechanical synergies between the hemitrichs and the core region in nonlinear regimes of deformations. The idealized model we present here therefore did not include branching of the rays, or details on the architecture of the hemitrichs (bone segments, hinges). There are several methods to solve beam problems subjected to large deflections and large rotations, for example elliptic integral solutions [31,32] or methods based on progressive softening of the structure [33]. For this work we used a nonlinear finite element modelling approach, which we found gave robust results at large deflections. The process of developing such a

model was highly instructive because it revealed some key features in terms of materials and geometries, as detailed below. A second use of the model is parameter identification. Here, we hypothesized that a model that captures key nonlinear mechanisms in the ray can be fitted onto the experiments to identify the properties of the different components of the ray. Fig. 5 shows the proposed model, with the main features as follows:

- The structure of the ray is idealized as a 2D model, where hemitrichs and core are modeled with linear elastic beam elements.
- The elements for the individual hemitrichs are linear elastic, with axial stiffness $(EA)_h$, flexural stiffness $(EI)_h$ and shear stiffness $(GA)_h$. Importantly, these properties were decoupled in the elements to capture the effect of segmentation. Although segmentation is not modeled explicitly in the models, the elements that model the hemitrichs could accept relatively high $(EA)_h$ combined with relatively low $(EI)_h$. The shear stiffness $(GA)_h$
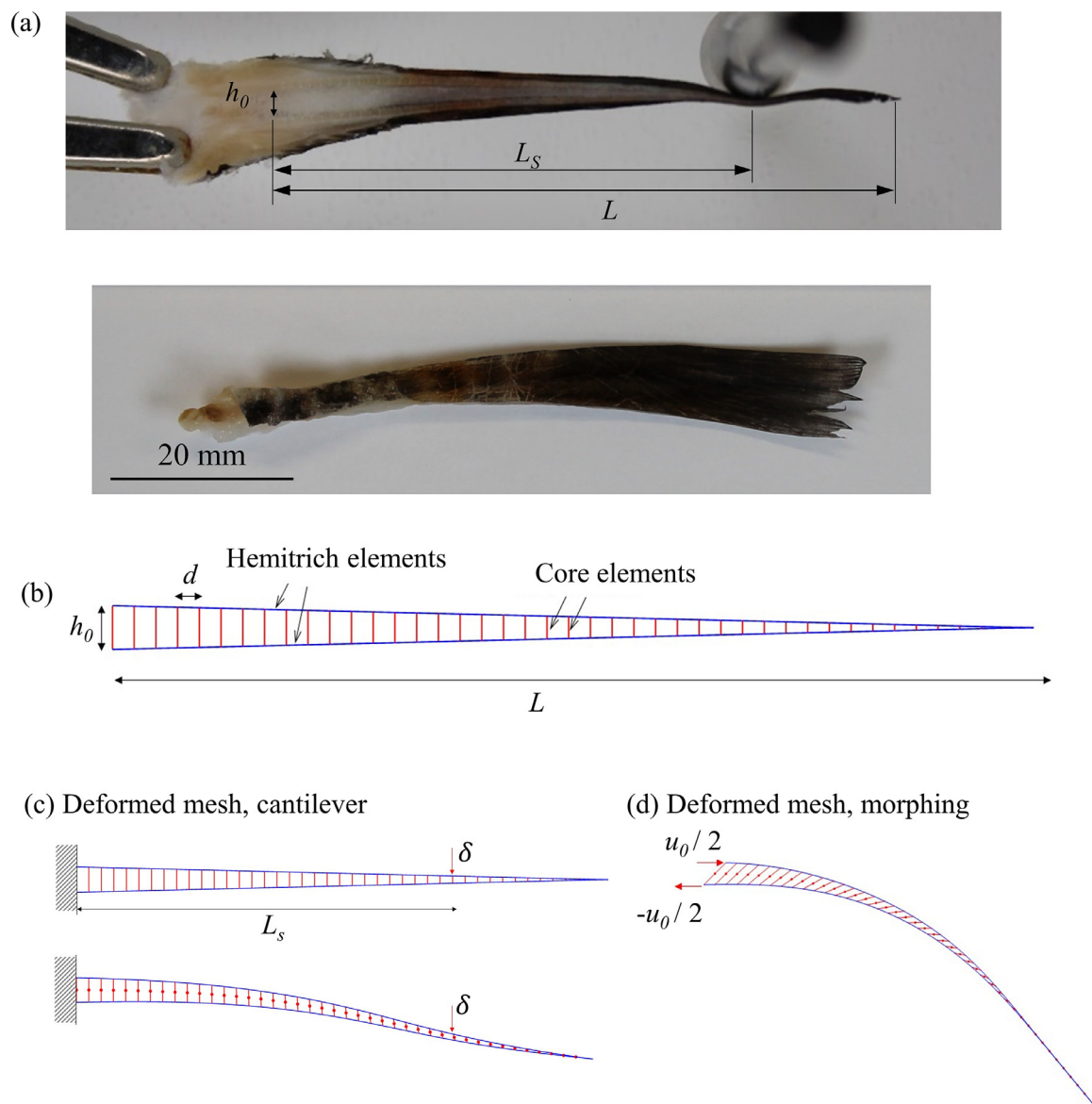

Fig. 5. Building a nonlinear finite element model for individual rays: (a) Typical images of an individual rays (top view and side view, in clamps). This type of images were used to measure key dimensions for the segmented region of the ray; (b) finite element model with co-rotational elements to capture the response of the hemitrichs (blue elements) and the core (red elements). This model can be subjected to (c) boundary conditions for cantilever loading or (d) boundary conditions for morphing.

had little effect on the results for the cantilever and morphing models.

- Non-linear, corotational beam elements [34,35] were used to capture geometrical nonlinearities at large deflections. In this formulation each node has three degrees of freedom (two displacements and one rotation).
- The overall geometry of the ray is linearly tapered, with the core region decreasing in thickness.
- The two hemitrichs are joined at the tip of the ray.
- The individual hemitrichs are tapered, with a cross section that decreases towards the end of the ray. The taper was not explicitly modeled, and instead a gradient of elastic properties was used for the hemitrichs. For simplicity we used a linear gradient, which is consistent with previous observations [6].
- Branching of the individual rays is a 3D feature of the individual rays (Fig. 2) which was not explicitly included in this 2D model. Instead, we assumed that once they branch, the mechanics of the branches can still be captured with a single set of hemitrichs as shown in the 2D model. In that sense, the properties of the branches are homogenized and "lumped" into a single ray. As shown below, this model still led to good agreements with the experiments, and provided useful insights into the properties of the rays.
- Our attempts to capture experiments using models with the core region as an isotropic elastic material were not successful, even at large deformations. Indeed, the core region is not isotropic, and its structure response is likely to be governed by the crimped collagen fibrils that connect the two hemitrichs. Since these fibrils can only carry tensile forces, we modeled the core region with an array of spring core elements (Fig. 5b). Each element captured the response of a large bundle of fibers, so their axial stiffness was written as wdE_c/h where w is the width of the ray (measured experimentally), E_c is the effective tensile modulus of the core region if it were stretched across the direction of the hemitrichs (this hypothesis is further developed below), and h is the length of the element, equal to the local thickness of the core. d is the spacing between the core elements, which is also the length for the hemitrich elements. d has no physical meaning and can be interpreted as the size of the finite element mesh.

This model was subjected to boundary conditions that simulate cantilever deflection from a transverse load (Fig. 5c), and morphing from actuation displacements at the base (Fig. 5d). For cantilever loading, the two nodes at the base of the model were clamped, and a transverse displacement δ was imposed at a distance L_s from the base. The reaction force at that point is the corresponding transverse force P. For morphing, one of the nodes was subjected to the actuation displacements $u_0/2$, and the other to - $u_0/2$, while rotation and vertical displacements were fixed to zero on both base nodes. With these boundary conditions, the point between the two base nodes is fixed and served as references for all positions. In terms of deformation, forces and mechanics, imposing $\pm u_0/2$ displacements on the two base nodes is identical to clamping one base node and imposing u_0 on the other, as it is done in the morphing experiments described above. The two solutions differ only by a rigid body displacement $u_0/2$. The horizontal reaction force at the two base nodes is the actuation force F_0. Before we present the results from these models, more details on the assumption of spring elements for the core will now be discussed in detail. Fig. 6a shows an idealized depiction of the core region between two hemitrichs. We assume that the mechanical behavior of the core is dominated by the collagen fibrils distributed transversely to the axis of the ray. Adjacent fibrils do not interact, and the effect of the soft matrix that surrounds the fibers is neglected (this type of extra-collagenous matrix is generally several orders softer than collagen fibrils). This fibrillar model for the core region produces mechanical responses which are completely different from previous models that assume a linear elastic response [3]. A pull across the axis of a ray with a fibrillar core (Fig. 6b) would result in the stretching of the fibrils along their axis. Assuming that individual fibrils are linear elastic, the overall tensile response of the core is governed by direct stretching of the fibers, so that the tensile force on the individual fibers is:

$$F_f = k_f \varepsilon_f \tag{1}$$

Where k_f is the tensile stiffness of the individual fibers. The homogenized stress and strains in the core region can also be written:

$$\begin{cases} \sigma_c = \rho F_f \\ \varepsilon_c = \varepsilon_f \end{cases} \tag{2}$$

Where ρ is the areal density of fibers. Eqs. (1) and (2) give:

$$\sigma_c = E_c \varepsilon_c \tag{3}$$

With $E_c = \rho k_f$ as the homogenized tensile modulus of the core region. Fig. 6b shows this simple linear response in tension. We now consider the shearing of the core region, as would happen during morphing and/or flexural deformations from transverse loads. Since the collagen fibrils are modeled as springs with negligible flexural and shear stiffness, the initial stiffness of the core in shear is zero. However, as shear deformations increase the fibrils stretch, rotate towards the shear direction, and produce forces along the direction of shearing (Fig. 5c). The elongation of the fibrils from shearing the core by a shear strain γ_c is:

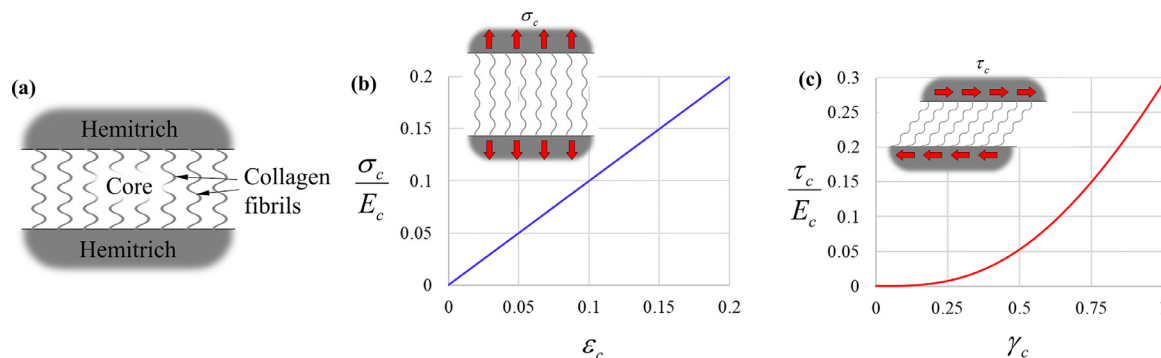$$\varepsilon_f = \sqrt{\gamma_c^2 + 1} - 1 \tag{4}$$

Fig. 6. Geometric stiffening of the core region: (a) The structure response of the core region is governed by collagen fibrils which connect the two hemitrichs; (b) If the fibrils are linear elastic spring, a hypothetical pull across the hemitrichs would result in a linear stress strain curve, with modulus E_c. E_c can be interpreted as the tensile modulus of the core along the direction of the fibrils; (c) When the same core region is sheared, the fibrils offer no resistance at small shear strains. At lager strains, the fibrils rotate and align with the shearing direction, producing stiffening.
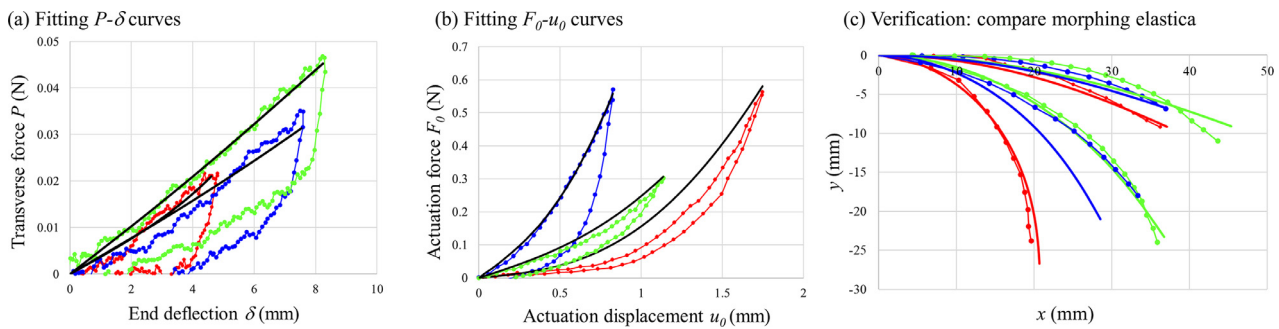
Fig. 7. Results the curve fitting procedure for three rays: (a) cantilever P-δ curve plot and (b) morphing F_0- u_0 curves (both experiments were fitted simultaneously for the same ray). The best fit from the model are shown with continuous black lines; (c) Verification of the model prediction with optimum structural parameters: Comparison between the morphing elastica predicted by the model and the experiments.

The individual fibers in turn produce tensile forces following Eq. (1). These forces are projected onto the shearing direction and then homogenized through the fiber density to give:

$$\frac{\tau_c}{E_c} = \left(1 - \frac{1}{\sqrt{1 + \gamma_c^2}}\right)\gamma_c \tag{5}$$

Fig. 6c shows the stress-strain curve of the interface in shear as predicted by Eqs. (4) and (5). The shear resistance of the core region is null at small deformation, but a strong nonlinear stiffening is generated as the fibers rotate, align and stretch in the direction of shearing. This effect also produces a normal stress across the core region which is not shown here, but which is captured in our finite element model.

4. Fitting the experimental data

We now use the numerical model described above to fit the experiments. We took the beginning of the segmented section of the ray as the origin for all coordinates. We also measured the displacement and rotation of this reference point and we removed them as rigid body displacements and rotations on the entire ray, so that after this procedure the reference point had no displacement or rotation. As a result, any possible deformations and rotations between the clamps and the start of the segmentation, or any other effects associated with the details of the clamping configuration were excluded from the fitting procedure. The model has three geometrical parameters: L, h_0 and w, which were all measured experimentally on each individual ray (Fig. 5a). L is the distance from the reference point to the end of the ray, h_0 is the distance between the hemitrichs at the reference point, and w is the average width of the ray. These measurements were different for each ray we tested and modeled. L ranged from about 36 to 54 mm, h_0 ranged from about 1.1 mm to 2.8 mm and w ranged from about 4.9 mm to 6.1 mm. We created a model for each ray based on the general model shown on Fig. 5b, but using the specific dimensions of each ray. We chose a mesh size $d = h_0$, which we found was small enough to reach mesh-independent results. The elements in the model have four structural properties: $(AE)_h$, $(EI)_h$, $(AG)_h$ and E_c. We found that $(AG)_h$ had little effect on the model over a wide range similar to $(AE)_h$, so it is fixed to $(AE)_h$ for the rest of this study. To fit the experiments, it was important to ensure that results were unique, and for this reason we followed this protocol: First, for a given ray, all dimensions were measured and a finite element model was built accordingly. The experimental P-δ curve and the experimental F_0-u_0 curves were then fitted simultaneously with the model, but only in the linear regime of small deformations. In this regime, the core region does not participate in the mechanical response (as shown on Fig. 6c), so we could obtain robust and unique values of the parameters $(AE)_h$ and $(EI)_h$ from the

fitting procedure. For simplicity we only used the loading curve of these experiments. The material model we use is rate independent and we did not consider the hysteresis seen in the experiments. The curve fitting was performed using a least-square optimization on a multi-objective function that sought to simultaneously minimize the sum of the experimental-model error for cantilever deflection and the experimental-model error for morphing (this optimization was performed using the *fminsearch* function on MATLAB). Using different initial guesses for the optimization invariably converged to the same optimum values $(AE)_h$ and $(EI)_h$, confirming that the solutions are unique for a given ray. In a second step, we considered the full experimental P-δ curves and experimental F_0-u_0 curves including large deflections. We used the $(AE)_h$ and $(EI)_h$ values obtained in the previous step, and this time we used the core modulus E_c as fitting parameter. Fig. 7 shows results from this fitting approach on experimental results from three rays. Although not perfect, the model properly captures the main features of the experiments including correct stiffnesses, a quasi-linear response in flexure, and stiffening behavior at large morphing actuations.

As a verification step, we also compared the elastica predicted by the model and the experiments for the morphing experiment. The model predictions, shown on Fig. 7c, show reasonable agreement with the experiments, which strengthen the results from the fitting procedure.

5. Results and implications for mechanics and bioinspiration

Fig. 8 shows the numerical results gathered using the fitting procedure on ten rays harvested from the caudal fins of three rainbow trout specimens in the form of bar plots, together with overall results given as mean ± standard deviation for each property. As expected, there are significant variations of properties across the rays we tested, even when variations in dimensions were considered. Repeatable property measurement therefore remains a challenge for fin rays, because of the large variability of ray properties within one fin, across different fins and across different fish species [6,28,30]. Nevertheless, the values we report here can still be used for comparisons, to learn about mechanics and to facilitate future translation to synthetic bioinspired structures. In their study on bluegill sunfish, Alben et al. [3] estimated the flexural stiffness $(EI)_h$ of the hemitrichs at 1 MPa.mm⁴, which compares well the values we report here. They estimated a shear modulus in the order of 10^3 Pa for the core region, but assuming a linear, isotropic and incompressible material [3]. In our model the tensile modulus of the core is 10-100 times greater, but our apparent shear modulus is infinitesimally small because of the way we modeled the core region with fibers. Despite large variations in results, $(AE)_h$, $(EI)_h$ and E_c have distinct and consistent magnitudes, which can be used to draw useful lessons from the construction and mechanics of the ray.
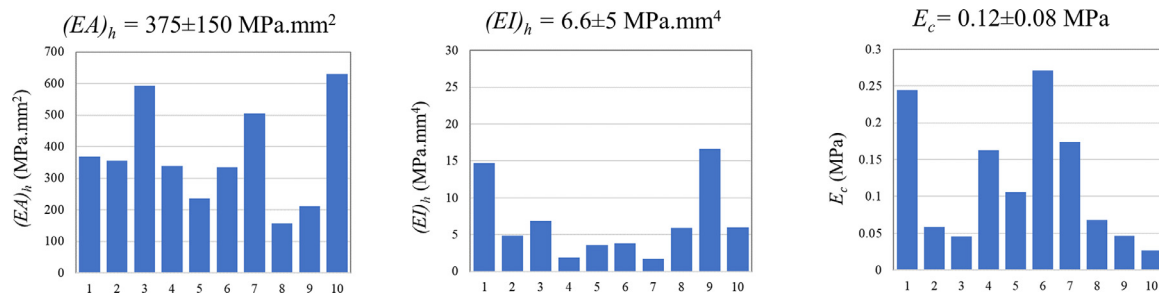
Fig. 8. Bar plots showing the results from curve fitting ten different fin rays. Overall results are given as mean ± standard deviation for each property. There is significant variability in the data, even after we considered variability in dimensions for each sample. Nevertheless, the results suggest broad trends when comparing these properties.

First, by considering the cross section of individual hemitrichs, it is possible to estimate their modulus. Fig. 9 shows a section (microCT) of the rays taken near the beginning of the segmented region. The section resembles a ring sector, and the data can be used to estimate the cross-sectional area $A_h \sim 0.25$ mm^2 and the second moment of inertia $I_h \sim 0.025$ mm^4. These values can then be used to estimate the modulus of the hemitrichs based on the results of Fig. 8. This procedure leads to an axial modulus $E_{h\ axial} \sim 1.5$ GPa and a flexural modulus $E_{h\ flexural} \sim 0.25$ GPa. These values are only apparent moduli, since the structure of the hemitrichs is segmented. However, the results make it clear that the axial stiffness of the hemitrichs is 5-6 times higher than the flexural stiffness. In terms of mechanics, this can be explained by the segmented architecture of the hemitrich. Compliant hinges at regular intervals along the hemitrichs provide low flexural stiffness, while maintaining high axial stiffness. In terms of functional benefits of such combination of properties, these results confirm the finding of our recent study on continuous and segmented 3D printed models of rays [5]. In essence, when the entire ray is deflected by a transverse force one of the hemitrich carries a compressive stress, while the other carries a tensile stress. The structural parameter that governs the flexural stiffness of the entire ray at small deflection is therefore the axial stiffness of the individual hemitrichs $(AE)_h$, (a result which is similar to the mechanics of I beams or composite panels with face sheets in engineering). To maximize flexural stiffness of the ray, the axial stiffness $(AE)_h$ must therefore be maximized. On the other hand, for efficient and rapid morphing of the ray, the force required for actuation must be minimized. Our previous study [5] has shown that minimizing the flexural stiffness $(EI)_h$ of the individual hemitrichs is key to maximizing this morphing efficiency. Achieving high $(AE)_h$ and low $(EI)_h$ simultaneously in individual hemitrichs is not possible with continuous structural beams with standard cross sections. Extreme combinations of high $(AE)_h$ and low $(EI)_h$ can however be achieved with structural segmentation, to maximize morphing efficiency. With estimates of the modulus of the hemitrichs in hand, we can also make comparisons with the modulus of the core region (Fig. 8c). Our results show that the stiffness of the hemitrichs is 3-4 orders of magnitude higher than the core. For efficient morphing distributed along the entire fin ray, the stiffness of the core region must be much smaller than the stiffness of the hemitrichs [3–5]. These results, based on nonlinear models and a reasonable representation of the core region as an array of elastic fibrils, represent to the best of our knowledge the most accurate estimate for the elastic properties of the core region.

Finally, the 2D model developed here can be used to explore the effects of key parameters on mechanical performance and functionality. In particular, one can demonstrate how the remarkable morphing and stiffness properties of natural rays result from finely tuned mechanical properties and mechanisms. For example, Fig. 10a shows a reference case where the fin ray properties found in Fig. 8 were assigned to the model. The morphing
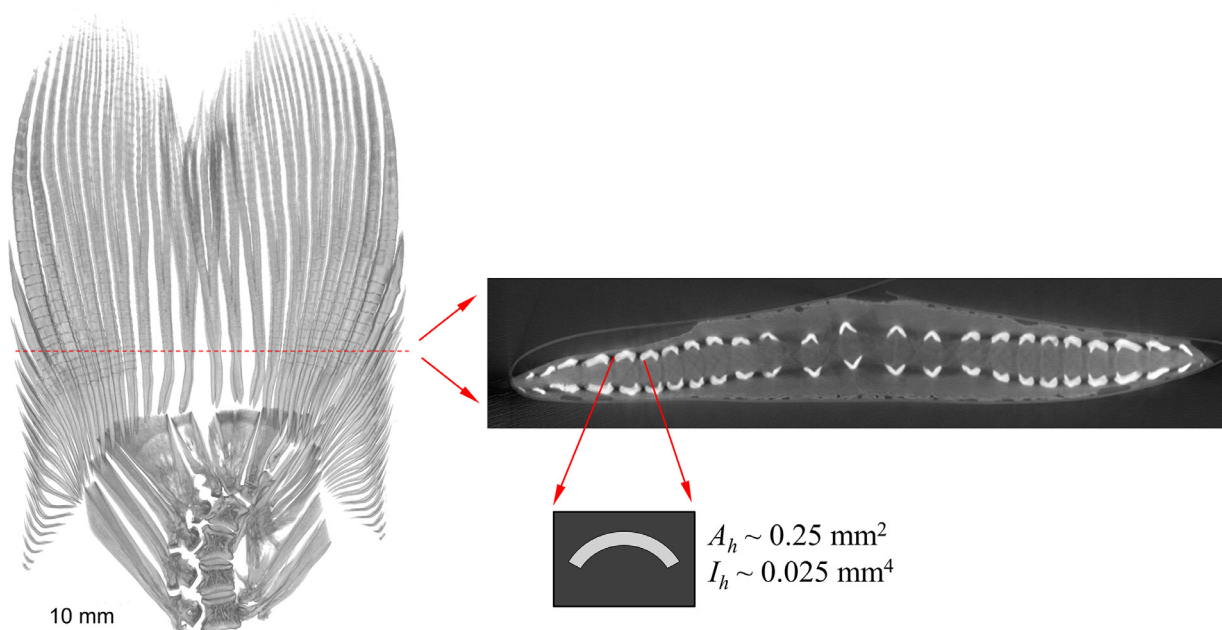

Fig. 9. Sections of the microCT data on the fin can be used to estimate the geometrical properties of the cross-section of individual hemitrichs.
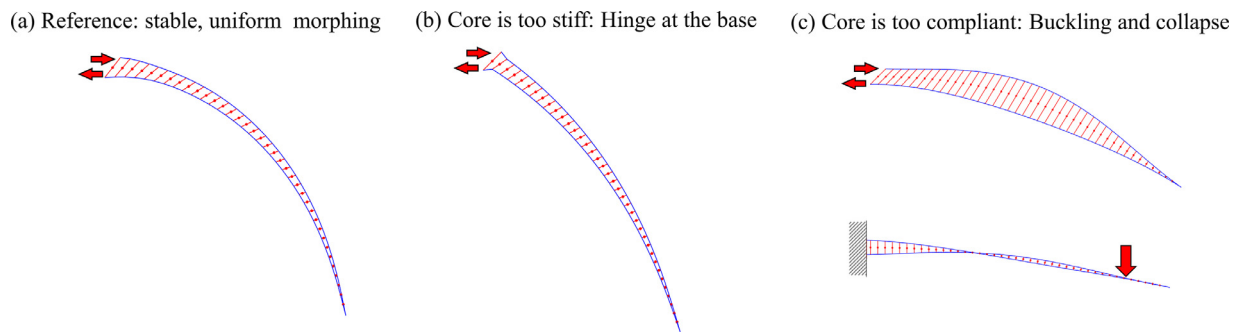
(a) Reference: stable, uniform morphing   (b) Core is too stiff: Hinge at the base   (c) Core is too compliant: Buckling and collapse

Fig. 10. The model can be used to assess the effect of the core region: (a) "proper morphing" predicted with the properties identified from the experiments; (b) case where the core is too stiff and where the deformations are concentrated near the base; (c) case where the core is too compliant which can lead to buckling or interpenetration of the hemitrichs.

response is uniform with a curvature distributed over the entire length of ray, and the structure is stable at large deformations. Fig. 10b shows the same model, but with the modulus of the core increased by three orders of magnitude. In this case the core region is too stiff compared to the hemitrichs and as a result the deformations are concentrated near the base, forming a localized "hinge". Fig. 10c shows another case, but this time with the modulus of the core decreased by three orders of magnitude compared to the reference case. In that case the hemitrich on the compressive side buckles at large deformations which limits morphing. In addition, the ray may collapse when subjected to transverse force at large deformations: in the case shown, the hemitrichs interpenetrate (this is a 2D model - there is no 3D twisting). These results show that while the fibrils in the core do not contribute to the mechanics of the ray at small deformations, they are critical to stabilize the ray at large deformations.

We finally ran a model where the two hemitrichs are separated at the end. These two hemitrich elements share a node in the regular models, and to separate these we simply modified their connectivity so they are disconnected. This "unfused" model produces the same results as the reference case, which confirms previous observations [3]: The core between the hemitrich is stiff enough to hold the two hemitrichs together and along their entire length during morphing and flexural deflections, so that the hemitrichs do not need to be physically fused at the end of the ray. The mechanics of morphing and stiffness are therefore robust, they are distributed over the entire length of the ray, and they can tolerate damage at the end of the ray.

6. Conclusions

The fin from ray-finned fish is a complex structure which provide high morphing capability combined with high stiffness. In this study, we have tested individual rays from the caudal fins of Rainbow trout, first under a transverse force to measure overall flexural response, and then under push-pull actuation at the base to generate morphing. In contrast with previous work which focused on small regime of deformation and linear regimes, we have considered large deflections, large rotations, and large shear strains in the core region, which was done through a 2D non-linear finite element model. In the process of developing this model and fitting the model onto the experiments, we have identified key structural properties that govern the morphing and flexural stiffness of the ray:

- Individual rays undergo large deflection and large rotations in normal conditions. Flexure and morphing of the ray can be captured with a 2D nonlinear model based on co-rotational beams.
- The flexural stiffness of the individual hemitrichs in the natural rays is 5-6 smaller than their axial stiffness. This contrast

is made possible by the segmented architecture of natural ray, and this combination simultaneously maximized flexural stiffness and morphing efficiency.
- The stiffness of the hemitrichs is 3-4 orders of magnitude larger than the stiffness of the core region in tension.
- The core region is composed of collagen fibrils that connect the hemitrichs. Accordingly, we showed that the core region can be modelled as an array of elastic fibers, as opposed to previous work which considered the core region as a linear elastic, homogenous material [3]. This fibrillar arrangement has profound implications in terms of mechanics: it allows for the extremely large shear deformations observed in the ray, it minimizes the force required to initiate morphing, it stiffens the ray at large deformation as a fail-safe mechanism and perhaps a tendon effect to maximize swimming efficiency. We also show that the fibrillar core is important to stabilize the ray at large deformations.
- Although more systematic studies would be needed in this regard, our preliminary results show that deviations from the properties identified on the natural ray led to sub-optimal morphing response and to unstable configurations at large deflections.
- Although more systematic studies would be needed in this regard, our preliminary results suggest that when the properties identified on the natural rays are used, the mechanical response of the ray is robust: clipping the end of the ray does not affect mechanical response.

Our experiments on the natural rays have also met two major difficulties: the mechanical response of the rays shows large variations across rays, even when they are taken from the same fin on the same fish. Our experiments have also shown significant viscoelastic effects, in the form of hysteresis in load-unload cycles, which we have not included in our model. There are therefore many opportunities to improve the accuracy of the experimental results and models, and to apply these methods to rays from other fins or from other fish species [36]. The 2D finite element model presented here was designed to capture the main structural features of individual rays, as well as their key deformation mechanisms and properties. Other features such as branching of the ray or the details of the architecture of the hemitrichs (bony segments, hinges) could be incorporated in more detailed, 3D finite element model at a higher computational cost, providing additional insight into this remarkable natural structure. Nevertheless, we believe that this study has shed a new light and new understanding of the properties and mechanics of the rays at large deformations, to a degree sufficient to attempt the design and fabrication of ray-inspired stiff morphing structures with large deformations that could be used for underwater propulsion [37–39], aerospace [40,41] or robotic "smart" materials [42–44].

Declaration of Competing Interest

The authors declare that they have no known competing financial interests or personal relationships that could have appeared to influence the work reported in this paper.

Acknowledgement

References

[1] J.J. Videler, Fish Swimming, Springer, Netherlands, Dordrecht, 1993.

[2] G.V. Lauder, Fish locomotion: recent advances and new directions, Ann. Rev. Mar. Sci. 7 (2015) 521–545, doi:10.1146/annurev-marine-010814-015614.

[3] S. Alben, P.G. Madden, G.V. Lauder, The mechanics of active fin-shape control in ray-finned fishes, J. R. Soc. Interface 4 (13) (2007) 243–256.

[4] P.J. Geerlink, J.J. Videler, The relation between structure and bending properties of teleost fin rays, Neth. J. Zool. 37 (1) (1987) 59.

[5] F. Hannard, M. Mirkhalaf, A. Ameri, F. Barthelat, Segmentations in fins enable large morphing amplitudes combined with high flexural stiffness for fish-inspired robotic materials, 6(57) (2021) eabf9710.

[6] B.R. Aiello, A.R. Hardy, C. Cherian, A.M. Olsen, C.P. Orsbon, M.E. Hale, M.W. Westneat, A comparison of pectoral fin ray morphology and its impact on fin ray flexural stiffness in labriform swimmers, J. Morphol. 279 (8) (2018) 1031–1044.

[7] C. Coulais, E. Teomy, K. de Reus, Y. Shokef, M. van Hecke, Combinatorial design of textured mechanical metamaterials, Nature 535 (2016) 529.

[8] P. Celli, C. McMahan, B. Ramirez, A. Bauhofer, C. Naify, D. Hofmann, B. Audoly, C. Daraio, Shape-morphing architected sheets with non-periodic cut patterns, Soft Matter 14 (48) (2018) 9744–9749.

[9] D. Restrepo, N.D. Mankame, P.D. Zavattieri, Phase transforming cellular materials, Extrem. Mech. Lett. 4 (2015) 52–60.

[10] E. Hawkes, B. An, N.M. Benbernou, H. Tanaka, S. Kim, E.D. Demaine, D. Rus, R.J. Wood, Programmable matter by folding, Proc. Natl. Acad. Sci. USA 107 (28) (2010) 12441–12445.

[11] Y. Cho, J.H. Shin, A. Costa, T.A. Kim, V. Kunin, J. Li, S.Y. Lee, S. Yang, H.N. Han, I.S. Choi, D.J. Srolovitz, Engineering the shape and structure of materials by fractal cut, Proc. Natl. Acad. Sci. USA 111 (49) (2014) 17390–17395.

[12] S.J. Jeon, A.W. Hauser, R.C. Hayward, Shape-morphing materials from stimuli-responsive hydrogel hybrids, Acc. Chem. Res. 50 (2) (2017) 161–169.

[13] E. Reyssat, L. Mahadevan, Hygromorphs: from pine cones to biomimetic bilayers, J. R. Soc. Interface 6 (39) (2009) 951–957.

[14] E. Siéfert, E. Reyssat, J. Bico, B. Roman, Bio-inspired pneumatic shape-morphing elastomers, Nat. Mater. 18 (1) (2019) 24–28.

[15] L. Guiducci, P. Fratzl, J.M. Bréchet Yves, W.C. Dunlop John, Pressurized honeycombs as soft-actuators: a theoretical study, J. R. Soc. Interface 11 (98) (2014) 20140458.

[16] A. Benjeddou, Shear-mode piezoceramic advanced materials and structures: a state of the art, Mech. Adv. Mater. Struct. 14 (4) (2007) 263–275.

[17] O.K. Rediniotis, L.N. Wilson, D.C. Lagoudas, M.M. Khan, Development of a shape-memory-alloy actuated biomimetic hydrofoil, J. Intell. Mater. Syst. Struct. 13 (1) (2002) 35–49.

[18] C. Thill, J. Etches, I. Bond, K. Potter, P. Weaver, Morphing skins, Aeronaut. J. 112 (1129) (2008) 117–139 (1968).

[19] B.R. Aiello, A.M. Olsen, C.E. Mathis, M.W. Westneat, M.E. Hale, Pectoral fin kinematics and motor patterns are shaped by fin ray mechanosensation during steady swimming in Scarus quoyi, J. Exp. Biol. 223 (Pt 2) (2020), doi:10.1242/jeb.211466.

[20] G.V. Lauder, J.L. Tangorra, Fish locomotion: biology and robotics of body and fin-based movements, in: R. Du, Z. Li, K. Youcef-Toumi, P. Valdivia y Alvarado (Eds.), Robot Fish: Bio-inspired Fishlike Underwater Robots, Springer Berlin Heidelberg, Berlin, Heidelberg, 2015, pp. 25–49.

[21] G. Liu, B. Geng, X. Zheng, Q. Xue, H. Dong, G.V. Lauder, An image-guided computational approach to inversely determine *in vivo* material properties and model flow-structure interactions of fish fins, J. Comput. Phys. 392 (2019) 578–593.

[22] B.E. Flammang, S. Alben, P.G.A. Madden, G.V. Lauder, Functional morphology of the fin rays of teleost fishes, J. Morphol. 274 (9) (2013) 1044–1059.

[23] S. Reddy N, S. Sen, C. Har, Effect of flexural stiffness distribution of a fin on propulsion performance, Mech. Mach. Theory 129 (2018) 218–231.

[24] N.K. Taft, B.N. Taft, Functional implications of morphological specializations among the pectoral fin rays of the benthic longhorn sculpin, J. Exp. Biol. 215 (15) (2012) 2703–2710.

[25] C.W. McCutchen, The trout tail fin: a self-cambering hydrofoil, J. Biomech. 3 (3) (1970) 271–281.

[26] B.R. Aiello, A.R. Hardy, C. Cherian, A.M. Olsen, S.E. Ahn, M.E. Hale, M.W. Westneat, The relationship between pectoral fin ray stiffness and swimming behavior in Labridae: insights into design, performance and ecology, J. Exp. Biol. 221 (1) (2018), doi:10.1242/jeb.163360.

[27] G.V. Lauder, P.G.A. Madden, R. Mittal, H.B. Dong, M. Bozkurttas, Locomotion with flexible propulsors: I. Experimental analysis of pectoral fin swimming in sunfish, Bioinspir. Biomim. 1 (4) (2006) S25–S34.

[28] S. Puri, T. Aegerter-Wilmsen, A. Jazwinska, C.M. Aegerter, *In vivo* quantification of mechanical properties of caudal fins in adult zebrafish, J. Exp. Biol. 221 (4) (2018) 7.

[29] L. Szewciw, F. Barthelat, Mechanical properties of striped bass fish skin: Evidence of an exotendon function of the stratum compactum, J. Mech. Behav. Biomed. Mater. 73 (2017) 28–37.

[30] B.R. Aiello, A.R. Hardy, C. Cherian, A.M. Olsen, S.E. Ahn, M.E. Hale, M.W. Westneat, The relationship between pectoral fin ray stiffness and swimming behavior in Labridae: insights into design, performance and ecology, J. Exp. Biol. 221 (1) (2018) jeb163360.

[31] A. Ohtsuki, F. Ellyin, Analytical approach to large deformation problems of frame structures. In case of a square frame with rigid joints, JSME Int. J. Ser. A 44 (2001) 89–93.

[32] A. Cammarata, M. Lacagnina, G. Sequenzia, Alternative elliptic integral solution to the beam deflection equations for the design of compliant mechanisms, Int. J. Interact. Des. Manuf. (IJIDeM) 13 (2) (2019) 499–505.

[33] F. Gao, W.H. Liao, X. Wu, Being gradually softened approach for solving large deflection of cantilever beam subjected to distributed and tip loads, Mech. Mach. Theory 174 (2022) 104879.

[34] K.J. Bathe, S. Bolourchi, Large displacement analysis of three-dimensional beam structures, Int. J. Numer. Methods Eng. 14 (7) (1979) 961–986.

[35] Y. Cai, J.K. Paik, S.N. Atluri, Large deformation analyses of space-frame structures, with members of arbitrary cross-section, using explicit tangent stiffness matrices, based on a von karman type nonlinear theory in rotated reference frames, CMES Comput. Model. Eng. Sci. 53 (2009) 123–152.

[36] J.T. Schaefer, A.P. Summers, Batoid wing skeletal structure: Novel morphologies, mechanical implications, and phylogenetic patterns, J. Morphol. 264 (3) (2005) 298–313.

[37] D. Quinn, G. Lauder, Tunable stiffness in fish robotics: mechanisms and advantages, Bioinspir. Biomim. 17 (1) (2022) 011002.

[38] C.J. Esposito, J.L. Tangorra, B.E. Flammang, G.V. Lauder, A robotic fish caudal fin: effects of stiffness and motor program on locomotor performance, J. Exp. Biol. 215 (1) (2012) 56–67.

[39] H. Liu, B. Taylor, O.M. Curet, Fin ray stiffness and fin morphology control ribbon-fin-based propulsion, Soft Robot. 4 (2) (2017) 103–116.

[40] S. Barbarino, O. Bilgen, R.M. Ajaj, M.I. Friswell, D.J. Inman, A review of morphing aircraft, J. Intell. Mater. Syst. Struct. 22 (9) (2011) 823–877.

[41] L. Zhao, Q. Huang, X. Deng, S.P. Sane, Aerodynamic effects of flexibility in flapping wings, J. R. Soc. Interface 7 (44) (2010) 485–497.

[42] G.V. Lauder, P.G.A. Madden, J.L. Tangorra, E. Anderson, T.V. Baker, Bioinspiration from fish for smart material design and function, Smart Mater. Struct. 20 (9) (2011).

[43] Z. Wolf, G.V. Lauder, A soft robotic model to study the effects of stiffness on fish-like undulatory swimming, in: D.A. Paley, N.M. Wereley (Eds.), Bioinspired Sensing, Actuation, and Control in Underwater Soft Robotic Systems, Springer International Publishing, Cham, 2021, pp. 153–169.

[44] Z. Liu, W. Sun, Z. Ren, K. Hu, T. Wang, L. Wen, A bio-inspired robotic fish fin with mechanosensation using conductive liquid-metal-infused soft actuators, in: Proceedings of the IEEE 9th Annual International Conference on CYBER Technology in Automation, Control, and Intelligent Systems (CYBER), 2019, pp. 689–694.